AIMS Energy, 13(4): 819–847.
DOI: 10.3934/energy.2025030
Received: 06 March 2025
Revised: 06 June 2025
Accepted: 01 July 2025
Published: 10 July 2025

https://www.aimspress.com/journal/energy

Research article

Experimental studies on the use of low catalyst loading in a proton exchange membrane fuel cell having twin inlet twin exit flow field

Sudesh Bekal[1,2,*]

[1] NITTE Deemed to be University, Mangaluru, India
[2] NMAM Institute of Technology, Nitte-574110, India

* **Correspondence**: Email: sudeshbekal@nitte.edu.in; Tel: +8904010966.

Abstract: A proton exchange membrane fuel cell (PEMFC) with reduced catalyst loading, specifically 0.2 mg/cm^2 at the anode and 0.4 mg/cm^2 at the cathode, was investigated using a twin inlet and twin outlet flow field configuration. The author conducted comparisons of voltage overpotential and maximum power output across various gas flow rates and humidification temperatures, contrasting these with results obtained from higher catalyst loading. Hydrogen flow rates of 80, 100, and 120 mL/min were utilized, with adjustments made to oxygen levels to achieve stoichiometric ratios, as well as 50%, 100%, and 150% excess oxygen. Notably, at a hydrogen flow rate of 100 mL/min, the maximum power output occurred at an oxygen flow rate of 125 mL/min. The optimal ratio of hydrogen to oxygen was further explored across different humidification temperatures ranging from 60 to 100 °C, inclusive of experiments conducted without humidification. Intermediate humidification temperatures yielded the best overall performance. We systematically assessed the voltage overpotential, maximum power point, and cell resistance under varying hydrogen-oxygen ratios and humidification temperatures. Our findings were compared with data obtained using higher catalyst loading configurations. The results obtained are validated by statistical analysis. The study demonstrates that the performance levels for reduced catalyst loading come close to that of higher catalyst loading configurations. Consequently, lower catalyst loading, which reduces the overall cost of the fuel cell, can be effectively employed in PEMFCs under specific operational parameters.

Keywords: lower catalyst loading; maximum power point; cell resistance; voltage overpotential; excess oxygen supply; humidification temperature

1. Introduction

Proton exchange membrane fuel cells (PEMFCs) are widely recognized as a promising technology for replacing fossil fuel-based systems in both stationary power generation and transportation [1–3]. However, several challenges, including the cost, durability, and effective management of water and heat, must be overcome before PEMFCs can be widely adopted across various applications [4,5]. Enhancing performance is crucial to reducing energy production costs, achievable in part through optimizing the flow field to improve water management and prevent flooding. Additionally, the flow field should ensure a uniform gas distribution across the membrane electrode assembly (MEA). Early designs employed a serpentine channel type of flow field due to its beneficial impact on fuel cells' performance [6,7]. Considerable experimental research has explored various novel bipolar plate designs.

For instance, Zhou et al. [8] explored opposite sinusoidal wave flow fields (OSWFFs) and intercepted flow fields (ICFFs), demonstrating improved performance compared with traditional parallel flow fields. Their studies indicated a 19% and 11% performance enhancement at 2.0 A/cm^2 for PEMFCs using single-inlet OSWFFs and ICFFs, respectively. Suarez et al. [9] conducted experiments across a wide range of operational conditions, analyzing polarization and power curves against a reference parallel-serpentine model. Their findings highlighted that a novel biomimetic design significantly improves water management, achieving a peak power output of 6.0% higher than the reference design. Another study [10] focused on the use of a special type of MPL based on plant root systems for effective drainage. Yet another study, Wang et al. [11], explored the active drainage flow field (ADFF) in comparison with the conventional serpentine flow field (CSFF). Their results indicated superior drainage performance for the ADFF due to under-rib flow and active drainage pressure, although both designs demonstrated comparable overall performance outputs.

The primary cost component of a fuel cell resides in the MEA, particularly the platinum catalyst it contains [12]. The cost of an MEA is directly influenced by the catalyst loading. Until a cost-effective alternative to platinum, offering comparable efficiency, is developed, platinum will remain indispensable in MEAs [13]. Even though other methods like ordered structures in the MEA [14] are used for improving the performance, appropriate use of platinum catalysts is essential for effective performance in PEMFCs. A platinum catalyst is essential for facilitating the electrochemical reactions at the anode and cathode. The reaction kinetics are influenced significantly by the catalyst loading. Even a slight reduction in platinum loading could lead to substantial cost savings.

This study investigates the performance implications of utilizing lower catalyst loadings along with a unique flow field design, aiming to achieve performance levels comparable with those achieved with higher platinum loadings. The bipolar plate employed in this research features two inlets and two outlets, strategically designed to maintain a uniform pressure distribution within the flow channels, thereby enhancing gas distribution.

Water management plays a crucial role in the primary function of the membrane, which is proton conduction. Maintaining a high water content within the membrane is critical. For thinner membranes, back diffusion of water may sufficiently counteract the drying effect at the anode caused by electroosmotic drag [15]. Fully humidifying both sides of the fuel cell has been shown to increase the maximum power output by approximately 50% compared with self-humidification methods [16]. The studies by Chen et al. [17] and Hung et al. [18] found that anode humidification has a more dramatic effect on PEMFCs' performance than oxygen humidification. Humidification of the anode is accomplished by the back diffusion of water. But where it is not sufficient, additional humidification of the anode is required. There is no recorded work which relates to experiments conducted on the special type of flow field with the catalyst concentration used in this study and also different humidification temperatures. In summary, an attempt has been made in this paper to experimentally determine the optimum values associated with the variables such as the hydrogen flow rate, excess oxygen supply, and the hydrogen humidification temperature for the fuel cell, which works with a combination of special type of bipolar plate and a lower catalyst load. The focus of the study is aimed at fuel cells for use in portable electronics with small requirement of power output.

2. Experimental methodology

The study investigated the performance of a proton exchange membrane fuel cell under two primary conditions: first, utilizing a lower catalyst loading and, second, employing a specialized type of flow field. The objectives are as follows:

(i) To examine the voltage overpotential, focusing on the activation loss, ohmic loss, and concentration loss under conditions of lower catalyst loading;

(ii) To investigate the maximum power point and cell resistance under conditions of lower catalyst loading;

(iii) To analyze the voltage overpotential and maximum power point across various humidification temperatures;

(iv) To compare these results with the optimal values obtained from configurations with higher catalyst loadings.

These investigations aimed to evaluate the impact of reduced catalyst loading and a unique flow field design on the performance metrics of the proton exchange membrane fuel cell.

2.1. Test conditions

In order to carry out the work, experiments have been conducted with the test condition shown in Tables 1 and 2.

The performance of the fuel cell was evaluated in terms of key output variables, specifically the maximum power output and the voltage overpotential. These output variables are primarily influenced by the current density, which was varied using an electronic load connected to the anode and cathode electrodes of the fuel cell.

In addition to current density, this study also considered several secondary independent variables that impact performance, namely the hydrogen gas flow rate and the level of excess oxygen. Although only one type of MEA with a lower catalyst loading was used in this study, the results

were compared with those from a previous study employing a higher platinum loading. This comparison aimed to determine whether a lower catalyst loading can achieve performance levels comparable with those of a higher catalyst loading.

Table 1. Test conditions for different hydrogen flow rates and excess oxygen supply with lower catalyst loadings.

MEA						
	Membrane: Nafion 212					
	Catalyst and catalyst support: Platinum and carbon paper					
	Catalyst loading: Low catalyst loadings of 0.2 mg/cm^2 (anode) and 0.4 mg/cm^2 (cathode)					
Bipolar plate						
	Flow field: Twin inlet, twin outlet serpentine					
	Material: Stainless steel					
Oxygen gas supply						
	Flow rate					
		for 80 mL/min hydrogen	40 mL/min	60 mL/min	80 mL/min	100 mL/min
		for 100 mL/min hydrogen	50 mL/min	75 mL/min	100 mL/min	125 mL/min
		for 120 mL/min hydrogen	60 mL/min	90 mL/min	120 mL/min	150 mL/min
	Excess oxygen		0%	50%	100%	150%
Humidification temperature						
	Hydrogen	60 °C				
	Oxygen	60 °C				

Table 2. Test conditions for different humidification temperatures at the best hydrogen flow rate and with excess oxygen supply.

MEA							
	Membrane: Nafion 212						
	Catalyst and catalyst support: Platinum and carbon paper						
	Catalyst loading: Low catalyst loadings of 0.2 mg/cm^2 (anode) and 0.4 mg/cm^2 (cathode)						
Bipolar plate							
	Flow field: Twin inlet, twin outlet serpentine						
	Material: Stainless steel						
Humidification temperature							
	Hydrogen	No humidification	60 °C	70 °C	80 °C	90 °C	100 °C
	Oxygen	No humidification	60 °C	60 °C	60 °C	60 °C	60 °C
Gas flow rate							
	Hydrogen	100 mL/min*					
	Oxygen	150% excess*					

*Note: These values are associated with the hydrogen flow rate and excess oxygen for the tests carried out as shown in Table 1.

Furthermore, an additional analysis was conducted to investigate the effect of hydrogen humidification temperature on the performance of a PEMFC with a reduced catalyst loading. These results were also compared with those obtained under higher catalyst loading conditions. In this analysis, while current density remains the primary controlling variable, the humidification temperature is also treated as a significant influencing factor.

In the experimentation conducted in this work, the MEA was provided with a carbon-supported platinum loading of 0.2 mg/cm^2 (anode) and 0.4 mg/cm^2 (cathode). In the author's earlier work, the platinum loading was 0.25 mg/cm^2 (anode) and 0.5 mg/cm^2 (cathode). The electrolyte used was Nafion 212 and was procured from Saienergy, India. The rate of the reduction reaction in the cathode was slow and to compensate for that, a higher amount of platinum was provided in the cathode electrode. Even a small reduction in platinum in the MEA would help in reducing the overall cost of the fuel cell and its operating cost. Hence, in this work, it was decided to reduce the platinum content in the MEA by 20%, and such an MEA was considered to have lower catalyst loading as against the higher catalyst loading of earlier studies carried out by the author.

The primary objective of this study was to evaluate the performance of a fuel cell operating with a specialized flow field and a low catalyst loading. Furthermore, we compare the optimal performance metrics obtained from previous research with higher catalyst loading against those achieved with a lower catalyst loading. This comparison aimed to determine whether the performance of the fuel cell with a lower catalyst loading could approximate that of configurations utilizing a higher catalyst loading.

To conduct the analysis, voltage output and power output values were recorded across different loads at intervals of 0.2 mA/cm^2. Loading ceased when the fuel cell could no longer sustain an increase in load.

The experiment comprised two distinct sets. (i) Under fixed values of humidification temperature and line temperature (referenced in Table 1), the fuel cell was loaded under varying hydrogen flow rates and excess oxygen supplies to determine the optimal settings. (ii) Using the optimal hydrogen flow rate and excess oxygen supply determined from the first set, experiments were then conducted at different humidification temperatures (referenced in Table 2) to establish the most suitable humidification temperature.

Using the data collected from the experiments, polarization curves and power output curves were plotted. From the polarization curves, various losses were identified, and from the power output curves, the maximum power points were determined. The voltage overpotential was determined from the polarization curve. The linear portion of the polarization curve was established by fitting a line to the data points corresponding to higher current density loads. The voltage drop in this linear segment of the curve indicates ohmic loss. Conversely, the voltage drop from the open circuit voltage to the beginning of the linear portion accounts for activation or kinetic loss.

Polynomial curve fitting was employed to derive models for the polarization curves. By differentiating these models, expressions for cell resistance were obtained.

In the first set of experiments, the maximum power point was determined for various levels of excess oxygen supply on the basis of the power output curves. These maximum power point values facilitate the identification of the load range at which high power output can be sustained. Additionally, the load range that permits a 10% decrease in maximum power output was established.

2.2. Experiment setup

The experimental setup comprised a fuel cell test station, a fuel cell unit, an electronic load, a computer workstation, and gas pipelines equipped with regulators and pressure gauges. Figure 1 illustrates the schematic diagram of this experimental setup.

The fuel cell test station has two humidifiers: One for hydrogen and one for oxygen humidification. Gas is supplied to the unit from a gas bank via a butterfly valve, pressure gauge, and flow regulators. The mass flow controller present in the test station precisely meters the gas according to user-defined values set in the software, delivering it to the appropriate humidifiers. Each humidifier is equipped with a heater whose temperature is controlled through the software interface.

The humidification temperature is regulated through the software dashboard installed on the computer. The recorded temperatures include the humidification temperatures for hydrogen (H_2) and oxygen (O_2), as well as the line temperatures for both gases. The computer interfaces with the master control unit of the fuel cell test station, which utilizes PID controllers. A PID (Proportional-Integral-Derivative) controller is an instrument used to regulate temperature, flow, in the fuel cell test station. These controllers adjust the heating elements on the basis of the discrepancy between the set point temperature and the actual temperature, integrating over time to minimize fluctuations. The electronic load utilized in the setup can handle a maximum current of 40 A and power levels of up to 400 W, allowing for precise loading of the fuel cell during experiments. The electronic loading unit features a display that indicates the voltage output, applied current, and power output.

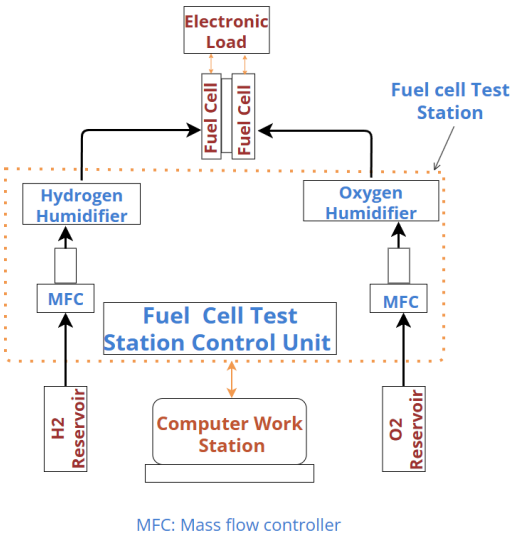

Figure 1. Schematic diagram of the experiment setup.

The conventional serpentine flow field has a serpentine channel running from inlet to outlet. While passing through the channel, the gas suffers from pressure drop due to Darcy-Weisbach losses and losses in the bends. This results in poor distribution of gases across the gas diffusion layer (GDL) and consequently, a loss in performance. The longer the flow field path, the higher these losses.

In the present work, an attempt has been made to shorten the flow field path's length while having the same overall path length. The design has two separate serpentine channels arranged so as to maximum the gas exposure area. Each channel has a separate inlet and outlet arranged in a manner

which ensures uniformity in the pressure even though Darcy-Weisbach losses still exist but of a lesser magnitude due to the shorter path length for each channel.

The fuel cell has a bipolar plate constructed from stainless steel (SS) and incorporates a specialized flow field design. This design includes two inlets and two outlet ports, facilitating separate channels. Figure 2 gives a visual representation of the bipolar plate. The overall dimensions of the bipolar plate are 10 cm × 10 cm. The flow field covers an area of 5 cm × 5 cm, perfectly accommodating an MEA with an equivalent active membrane area. Within this flow field, there are two channels: One measuring 567 mm and the other 467 mm in length. These channels are arranged so that gas enters each channel through dedicated inlets and travels a significant distance before exiting through dedicated outlets. The objective is to divide the overall flow path into two distinct channels. By reducing the path length, the pressure loss in each channel is lower than it would be in a single channel with a total length equal to the sum of the two separate channels. This configuration promotes a uniform distribution of gases. The inlets of the two channels are offset by a distance of 150 mm.

In the first channel, gas flow over an initial length of 100 mm results in a specific pressure drop. At this point, the gas enters the inlet of the second channel. Rim convection facilitates a flow from the second channel back into the first, partially restoring its pressure. Consequently, the pressure of the gas in both channels equalizes at this juncture. The channels then run parallel to each other, ensuring a uniform pressure distribution across the MEA.

As depicted in Figure 3, the gas from the first channel exits 100 mm before the gas from the second channel. This additional distance travelled by the gas in the second channel leads to a continuous pressure drop. This phenomenon aids in displacing a certain amount of moisture present within the channel. Therefore, this type of flow field not only helps to maintain a uniform pressure across the majority of the MEA but also facilitates the removal of excess moisture. This design is expected to enhance the fuel cell's performance significantly, even with reduced catalyst loading, by minimizing pressure losses and optimizing the gas distribution within the cell.

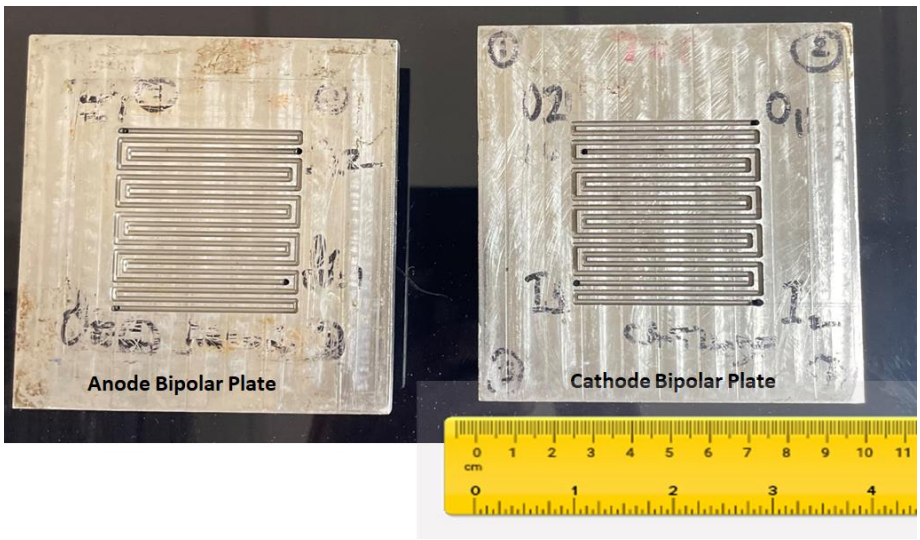

Figure 2. Anode and cathode bipolar plates (material: SS; overall size: 10 cm × 10 cm; flow field area: 5 cm × 5 cm; channel size: 1.5 mm width, 1.5 mm depth, 1 mm rim width; channel length for Channel 1: 567 mm; channel length for Channel 2: 467 mm).

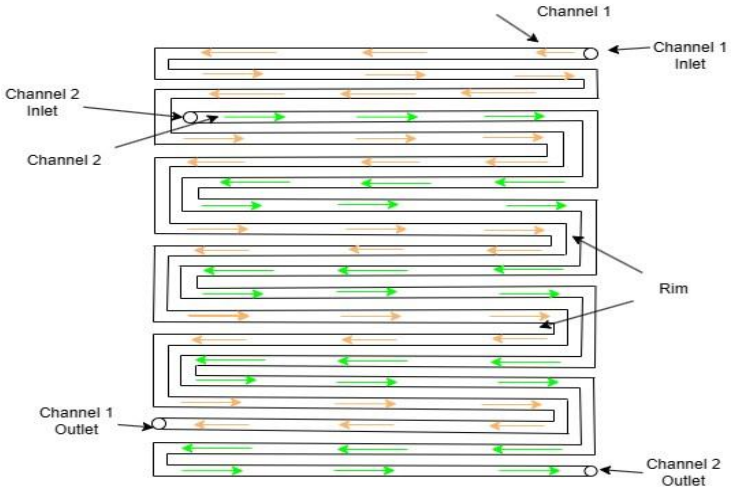

Figure 3. Flow of gas in the channels (green arrow: Flow in Channel 2; brown arrow: Flow in Channel 1).

3. Results and discussion

The objective of this study was to find out how changes in the humidification temperature, hydrogen flow rate, and excess oxygen supply affect the voltage overpotential and maximum power point. The experiments were conducted using a low platinum catalyst loading and a specialized bipolar plate having twin inlet and twin outlet openings. The aim was to understand how the variables influence the performance of the fuel cell under a specific platinum catalyst loading and with the use of bipolar plate as mentioned above. The fuel cell under consideration here is without external heating, and hence the power output is limited to 700 mW and the current density is limited to 100 mA/cm^2. The results obtained from this research are useful for fuel cells used in portable electronics where external heating will add to the unit cost and hence is best avoided.

3.1. Comparison of voltage overpotential for different hydrogen flow rates and excess oxygen supply

The oxygen flow rate was varied according to each hydrogen flow rate of 80, 100, and 120 mL/min. The variation in the oxygen flow rate was adjusted to achieve excess oxygen levels of 0%, 50%, 100%, and 150%. Figure 4 illustrates the voltage output variations for different hydrogen flow rates: Figure 4(A) shows the voltage output for a 80 mL/min hydrogen flow rate, Figure 4(B) for 100 mL/min, and Figure 4(C) for 120 mL/min.

It was noted that a 100% excess oxygen supply resulted in the lowest voltage overpotential for hydrogen flow rates of 80 mL/min and 120 mL/min. Conversely, for the 100 mL/min hydrogen flow rate, the minimum voltage overpotential was associated with a 150% excess oxygen supply.

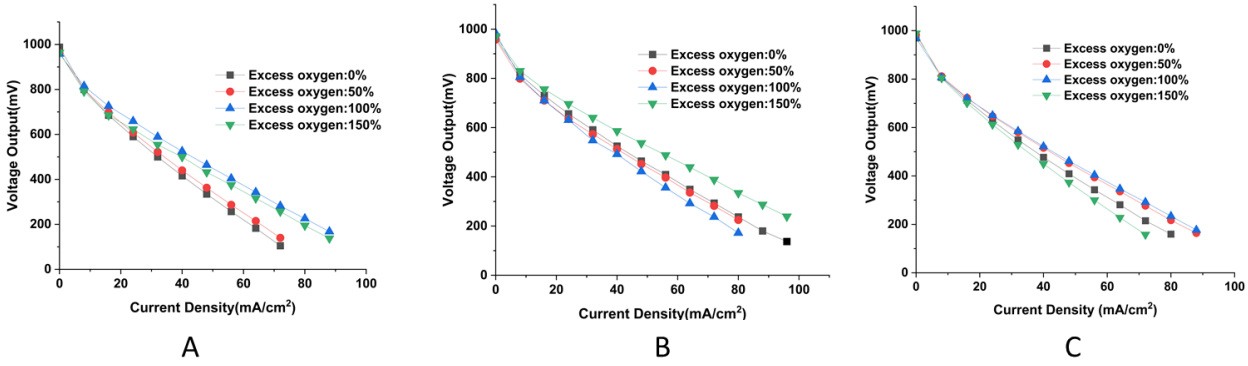

Figure 4. Variation in voltage output for different loads at various excess oxygen levels and hydrogen flow rates. A: Hydrogen flow rate of 80 mL/min. B: Hydrogen flow rate of 100 mL/min. C: Hydrogen flow rate of 120 mL/min.

Table 3 displays the various losses for different hydrogen flow rates and percentages of excess oxygen. Upon comparing the activation and ohmic losses with the stable operating polarization curve, it becomes evident that activation losses significantly influence the stability of the polarization curve, correlating with the minimal voltage output drop.

Table 3. Voltage overpotential for different hydrogen flow rates and excess oxygen levels.

	Activation loss				Ohmic loss				Concentration loss			
Excess oxygen	0	50	100	150	0	50	100	150	0	50	100	150
80 mL/min hydrogen	572	523	433	532	311	300	357	294	0	0	0	0
100 mL/min hydrogen	439	385	435	331	388	348	376	450	0	0	0	0
120 mL/min hydrogen	493	467	448	539	317	352	345	292	0	0	0	0

For the 80 mL/min hydrogen flow rate depicted in Figure 4(A), the stable curve corresponds to a 100% excess oxygen supply. From Table 3, it is noted that the activation loss is lowest (433 mV) for this flow rate, specifically at 100% excess oxygen, and there is not much variation in the ohmic losses. The total voltage overpotential is also minimum (790 mV) under these conditions, as mentioned earlier.

For the 100 mL/min hydrogen flow rate, the lowest activation loss (331 mV) is observed at 150% excess oxygen, coinciding with the lowest total voltage overpotential (781 mV). It should be noted that although 50% excess oxygen shows the least total voltage overpotential (733 mV), the fuel cell's load capacity is limited (terminating around 80 mA/cm² current density). With 150% excess oxygen, the polarization curve extends beyond 100 mA/cm², thus demonstrates a good load-carrying capacity.

Regarding the 120 mL/min hydrogen flow rate, both the 50% and 100% excess oxygen levels exhibit minimal activation losses. However, these conditions result in lower load capacity, failing to exceed the 90 mA/cm² current density. The fuel cell, when operated with this special type of bipolar plate and lower catalyst concentration, need to run at an excess oxygen supply of 100% or more for any hydrogen flow rate considered in the study while keeping the limited current density at the highest.

Interestingly, as depicted in Figure 4, the tail ends of the polarization curves show no bending, suggesting the absence of concentration losses. In contrast, our previous studies with a higher catalyst loading under similar conditions showed significant concentration losses (200–300 mV). Higher catalyst loadings tend to consume oxygen more rapidly during its initial passage through the channels, leading to oxygen deficiency in the later portions of the flow field.

3.2. Comparison of maximum power points for different hydrogen flow rates and excess oxygen supply

The power output of a fuel cell serves as a key indicator of its efficiency. Figure 5 illustrates the variation in power output with load for different hydrogen flow rates and levels of excess oxygen.

As the load (current density) increases, the voltage output decreases due to the onset of activation losses, ohmic losses, and concentration losses at different stages of applied load. Initially, the power output rises because the increase in applied load outpaces the decline in voltage output. For instance, at the 120 mL/min hydrogen flow rate and 150% excess oxygen, when the load increases by 200%, voltage output decreases by 23% at lower loads. However, as the load continues to increase, the decline in voltage surpasses the increase in load. In the earlier example, for higher load regions, while the load increases by 23%, the voltage output decreases by 47%, causing the power output curve to dip.

During the ohmic loss phase, these two values—load increase and voltage decrease—remain relatively close in magnitude but opposite in direction. This balance results in a plateau in the power output curve.

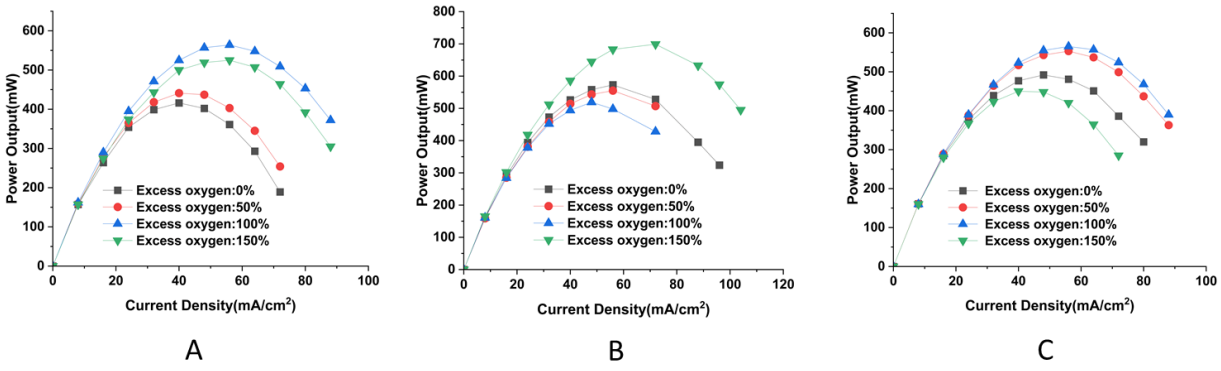

Figure 5. Power output trends for different loads at various excess oxygen levels and hydrogen flow rates. A: Hydrogen flow rate of 80 mL/min. B: Hydrogen flow rate of 100 mL/min. C: Hydrogen flow rate of 120 mL/min.

When plotting the graphs in Figure 5, the curve terminates at the point where the fuel cell can no longer sustain an increase in load, as indicated by no change in the current despite attempts to further increase it, even though the voltage output remains above zero. This current density is called the limiting current density as it restricts the load-bearing capacity of the fuel cell.

In applications such as serving as a prime-mover in transportation systems or in portable electronics, fuel cells encounter continuous variations in load. Specific load requirements can be met

by generating adequate power through suitable hydrogen flow rates and excess oxygen supply. In the same way, to achieve maximum power generation for improved efficiency, the excess oxygen supply and/or hydrogen flow rate need necessary adjustments. For instance, in Figure 5A, to meet a load requirement of 62 mA/cm², a minimum power output of approximately 280 mW is achieved with 0% excess oxygen supply. However, to enhance fuel cells' efficiency, a higher power output of around 350 mW can be achieved by supplying 50% excess oxygen. Consistently operating the fuel cell at its peak efficiency involves tracking the maximum power point (MPP). This can be accomplished by either adjusting the load while maintaining a constant hydrogen flow rate and excess oxygen supply, or by adjusting the hydrogen flow rate and excess oxygen supply while keeping the load constant. This approach ensures optimal performance and efficiency across varying operational conditions.

Table 4 presents the maximum power at the maximum power point (MPP), along with the corresponding hydrogen flow rate and excess oxygen levels. The MPP covers a load range from 40 to 64 mA/cm². To encompass a broader range of load conditions, a 10% decrease in power output was applied, and the resulting power outputs along with their corresponding hydrogen flow rate and excess oxygen supply values are also detailed in Table 4.

Upon allowing for a 10% reduction in power output, the load range expands to 32–80 mA/cm², compared with the narrower 40–60 mA/cm² range covered by the power outputs at MPP. Achieving optimal efficiency requires the fuel cell to track the MPP. However, even with the setup and methodology employed in this study, the range of load conditions covered remains relatively narrow.

Future research efforts should therefore focus on expanding the load range that encompasses the MPPs, especially if minimizing power loss is a primary objective. This expansion would enhance the fuel cell's capability to operate efficiently across a wider spectrum of operational conditions.

Figure 5A, plotted for a hydrogen flow rate of 80 mL/min, illustrates that at low levels of excess oxygen (0% and 50%), the MPP is low, corresponding to a load of 40 mA/cm². This is due to the combined effect of insufficient hydrogen and oxygen flow rates, resulting in diminished power output.

Increasing the excess oxygen level to 100% enhances the reaction at the cathode, thereby reducing the activation losses, as depicted in Figure 4. Consequently, this leads to higher power generation (564 mW) at a higher load value (56 mA/cm²). However, further increasing the excess oxygen to 150% causes a decrease in power at the MPP while maintaining the same load value. Analysis of Figure 4 shows that while the ohmic loss slope remains consistent for both the 100% and 150% excess oxygen levels, there is an increased activation loss at 150%, likely due to the oxygen quenching effect on the cathodic reaction, resulting in a 6% reduction in maximum power output.

Table 4. Maximum power, hydrogen flow rate, and excess oxygen supply at the MPP and a 10% decrease in the MPP.

Current density	At the MPP			At a 10% decrease in the MPP		
	Max. power (mW)	H_2 flow rate (mL/min)	Excess oxygen (%)	Max. power (mW)	H_2 flow rate (mL/min)	Excess oxygen (%)
32				399/418/423	80/80/120	0/50/150
40	416	80	0	416/441/450/525/500/526/514/494/477/517/523	80/80/120/80/80/100/100/100/120/120/120	0/50/150/100/150/0/50/100/0/50/100
	441	80	50			
	450	120	150			
48	519	100	100	519/492/402/437/557/519/558/543/645/543/555/448	100/120/80/80/80/80/100/100/100/120/120/120	100/0/0/50/100/120/0/50/150/50/100/150
	492	120	0			
56	564	80	100	564/525/573/555/553/565/403/508/683/481/420	80/80/100/100/120/120/80/100/100/120/120	100/150/0/50/50/100/50/100/150/0/150
	525	80	150			
	573	100	0			
	555	100	50			
	553	120	50			
	565	120	100			
64	704	100	150	704/548/507/561/537/479/451/557	100/80/80/100/100/100/120/120	150/100/150/0/50/100/0/100
72				509/528/507/699/499/524	80/100/100/100/120/120	100/0/50/150/50/100
80				670	100	150

At a hydrogen flow rate of 100 mL/min, the power at MPP for 0%, 50%, and 100% excess oxygen levels are closely grouped, while 150% excess oxygen produces 22% more power compared with the next best MPP. This is attributed to the additional hydrogen protons and oxygen facilitating a faster reaction rate.

With a hydrogen flow rate of 120 mL/min, the maximum power output increases with the excess oxygen level. However, at 150% excess oxygen, the maximum power decreases by 20% compared with the next best value at 100% excess oxygen. Figure 4 indicates an increase in activation loss at this excess oxygen level, likely due to excess water production at the cathode slowing down the reaction rate.

In summary, optimizing the hydrogen flow rate and excess oxygen level is crucial for achieving maximum power efficiency in fuel cells, with excess oxygen levels significantly influencing activation and ohmic losses, thereby impacting the overall power output.

3.3. Comparison of cell resistance for different excess oxygen supply and hydrogen flow rates

The voltage and power output of a PEMFC are known to fluctuate in response to changes in the cell's resistance, which can be influenced by factors such as moisture levels and flow rates.

Investigating how the hydrogen flow rate and excess oxygen level affect cell resistance is particularly intriguing.

Due to the unavailability of equipment for directly measuring the cell's resistance and the limitations of the test station used, alternative methods were employed for calculation.

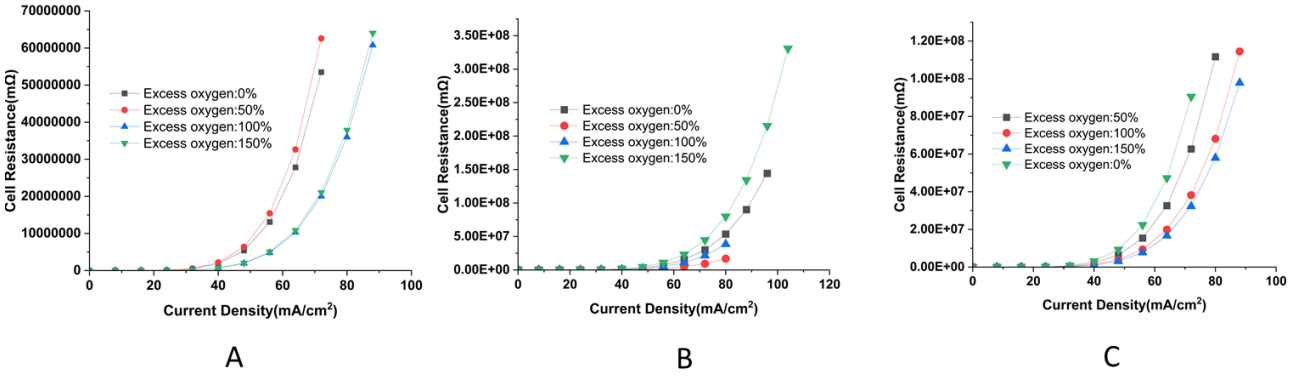

Figure 6. Variation in the cell's resistance for different loads at various excess oxygen levels and hydrogen flow rates for a lower catalyst loading. A: Hydrogen flow rate of 80 mL/min B: Hydrogen flow rate of 100 mL/min. C: Hydrogen flow rate of 120 mL/min.

The cell resistance for this study was obtained by differentiating the models developed on the basis of the sixth-degree polynomial best fit representing all polarization curves. The following are the expressions for cell resistance.

For the 80 mL/min hydrogen flow rate

With 0% excess oxygen:

$$\text{Cell resistance (m}\Omega) = 0.045J^5 - 1.492J^4 + 19.05J^3 - 117.108J^2 + 350.7J - 502.88, \quad (1)$$

where J is the current density (mA/cm^2).

With 50% excess oxygen:

$$\text{Cell resistance (m}\Omega) = 0.0516J^5 - 1.6425J^4 + 20.0432J^3 - 117.087J^2 + 330.46J - 450.34. \quad (2)$$

With 100% excess oxygen:

$$\text{Cell resistance (m}\Omega) = 0.018J^5 - 0.671J^4 + 9.5528J^3 - 65.553J^2 + 218.08J - 348.22. \quad (3)$$

With 150% excess oxygen:

$$\text{Cell Resistance (m}\Omega) = 0.0192J^5 - 0.7374J^4 + 11.0372J^3 - 80.172J^2 + 282.92J - 449.81. \quad (4)$$

For the 100 mL/min hydrogen flow rate

With 0% excess oxygen:

$$\text{Cell resistance (m}\Omega) = 0.0258J^5 - 0.8965J^4 + 12.204J^3 - 81.015J^2 + 264.66J - 405.48. \quad (5)$$

With 50% excess oxygen:

$$\text{Cell resistance (m}\Omega) = 0.009J^5 - 0.377J^4 + 6.1512J^3 - 48.237J^2 + 181.978J - 316.42. \quad (6)$$

With 100% excess oxygen:

$$\text{Cell resistance (m}\Omega) = 0.0192J^5 - 0.714J^4 + 10.2328J^3 - 70.18J^2 + 232.44J - 365.16. \quad (7)$$

With 150% excess oxygen:

$$\text{Cell resistance (m}\Omega) = 0.0384J^5 - 1.3245J^4 + 17.5748J^3 - 111.906J^2 + 345.44J - 489.9. \quad (8)$$

For the 120 mL/min hydrogen flow rate

With 0% excess oxygen:

$$\text{Cell resistance (m}\Omega) = 0.0522J^5 - 1.693J^4 + 20.888J^3 - 123.105J^2 + 350.4J - 468.31. \quad (9)$$

With 50% excess oxygen:

$$\text{Cell resistance (m}\Omega) = 0.033J^5 - 1.178J^4 + 16.1188J^3 - 105.633J^2 + 333.64J - 475.74. \quad (10)$$

With 100% excess oxygen:

$$\text{Cell resistance (m}\Omega) = 0.0288J^5 - 1.059J^4 + 14.8J^3 - 98.679J^2 + 315.32J - 452.77. \quad (11)$$

With 150% excess oxygen:

$$\text{Cell resistance (m}\Omega) = 0.0738J^5 - 2.301J^4 + 27.6896J^3 - 160.266J^2 + 448.8J - 573.58. \quad (12)$$

Using the equations provided, cell resistance was computed and the resulting values are depicted against current density in Figure 6. At a hydrogen gas flow rate of 80 mL/min, the maximum power point (MPP) was observed at load values of 40, 40, 56, and 48 mA/cm², respectively, for 0%, 50%, 100%, and 150% excess oxygen supply. Figure 6A reveals that the cell resistance curves maintain near-asymptotic behavior with the current density up to approximately 40–50 mA/cm² across all conditions.

Interestingly, it was observed that cell resistance remains relatively stable until reaching the MPP; beyond this point, an increase in load leads to an increase in cell resistance. Under specific experimental conditions, cell resistance can vary depending on the conductivity of the MEA, which itself is influenced by humidity levels, as depicted in Figure 7. This figure illustrates different humidification temperatures ranging from no humidification to 100 °C for hydrogen gas.

For instance, at a constant load of 80 mA/cm², as shown in Figure 7A, the cell resistance increases with an increase in the hydrogen humidification temperature, with the highest resistance observed at both no humidification and 100 °C humidification temperatures. The differences in cell resistance at other humidification temperatures are minimal. The reaction at the cathode produces water, some of which is transported to the anode by back diffusion, some of which depends on the concentration of water in the anode. Additionally, the water is also carried from the anode to the cathode by the protons through electro-osmotic drag. At a humidification temperature of 100 °C, these activities become more vigorous. The presence of excess water in the anode and cathode act as an impediment for the flow of electrons, thus causing increase in the cell's resistance. Under no humidification on the anode side and normal humidification with a humidification temperature of 60 °C on the cathode, the presence of voids in the anode offer resistance to the flow of electrons. Hence, the cell's resistance is high. Moreover, even with a higher catalyst loading, the cell's resistance increases with the humidification temperature. While for the lower catalyst loading, the cell's resistance remains asymptotic until around 40 mA/cm², where it extends to approximately 65 mA/cm²

with a higher catalyst loading. For the same load (say, 45 mA/cm^2), the electrons produced are the same in both cases. However, in the case of the higher catalyst loading, a larger reaction area is available and hence the density of electrons is less for the higher catalyst loading. Consequently, this results in less overall resistance in the cell. Notably, the cell's resistance under zero humidification and a 100 °C humidification temperature is higher for the lower catalyst loading compared with the higher catalyst loading scenarios.

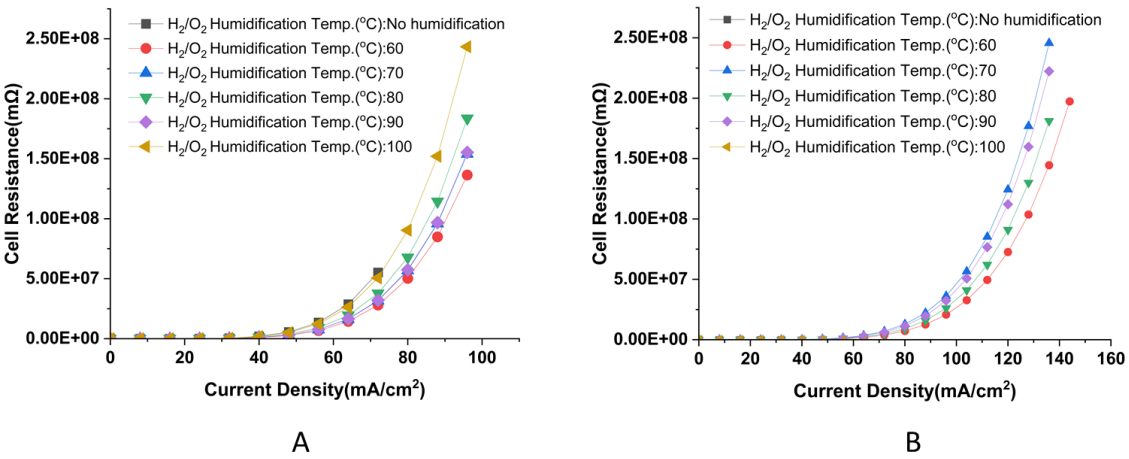

Figure 7. Variation in the cell's resistance with humidification temperature. A: Low catalyst loading. B: High catalyst loading.

The expression for the cell's resistance for different hydrogen humidification temperatures are given below for the lower catalyst loading.

$$\text{Cell resistance for zero humidification} = 0.0462J^5 - 1.514J^4 + 19.19J^3 - 117.549J^2 + 350.9J - 497.16; \quad (13)$$

$$\text{Cell resistance for 60 °C} = 0.0252J^5 - 0.9435J^4 + 13.478J^3 - 92.082J^2 + 301.04J - 443.07; \quad (14)$$

$$\text{Cell resistance for 70 °C} = 0.0282J^5 - 1.0355J^4 + 14.592J^3 - 98.283J^2 + 317.3J - 462.28; \quad (15)$$

$$\text{Cell resistance for 80 °C} = 0.0336J^5 - 1.2295J^4 + 17.1252J^3 - 114.039J^2 + 364.12J - 515.85; \quad (16)$$

$$\text{Cell resistance for 90 °C} = 0.0282J^5 - 1.014J^4 + 13.9592J^3 - 92.22J^2 + 294.38J - 433.56; \quad (17)$$

$$\text{Cell resistance for 100 °C} = 0.0432J^5 - 1.4695J^4 + 19.2072J^3 - 121.041J^2 + 369.44J - 512.12. \quad (18)$$

The expression for the cell's resistance for different hydrogen humidification temperatures are given below for the higher catalyst loading.

$$\text{Cell resistance for Zero humidification} = 12.4286J - 207.39; \quad (19)$$

$$\text{Cell resistance for 60 °C} = 0.0048J^5 - 0.267J^4 + 5.332J^3 - 48.975J^2 + 206.92J - 368.65; \quad (20)$$

$$\text{Cell resistance for 70 °C} = 0.0078J^5 - 0.395J^4 + 7.608J^3 - 67.578J^2 + 275.48J - 457.21; \quad (21)$$

$$\text{Cell resistance for 80 °C} = 0.006J^5 - 0.332J^4 + 6.6204J^3 - 60.897J^2 + 257.7J - 446.56; \quad (22)$$

$$\text{Cell resistance for 90 °C} = 0.0072J^5 - 0.3795J^4 + 7.2776J^3 - 64.485J^2 + 263.08J - 443.17; \quad (23)$$

$$\text{Cell resistance for 100 °C} = -0.1685J^4 + 5.3416J^3 - 58.356J^2 + 261.84J - 481.68. \quad (24)$$

3.4. Comparison of voltage overpotential for different humidification temperatures

In the context of the lower catalyst loading, the authors aimed to investigate the impact of varying hydrogen gas humidification temperatures on the voltage overpotential. The investigation was carried out for the hydrogen flow rate and excess oxygen supply which resulted in the best maximum power output. Figure 8 illustrates the voltage output across different loads while adjusting the hydrogen gas humidification temperature from 60 °C to 100 °C in 10 °C increments, while maintaining the oxygen gas humidification temperature at 60 °C. The polarization curves for 60 °C, 70 °C, 80 °C, and 90 °C are closely grouped together, with the 90 °C humidification temperature showing superior performance.

The results from the conditions of no humidification and the highest tested humidification temperature (100 °C) demonstrate poorer performance, similar to the findings observed with the higher catalyst loading. Specifically, the excessively high humidification temperature (100 °C) leads to flooding in the cathode's flow field channels, whereas the absence of humidification results in inadequate proton transport across the membrane. Both scenarios contribute to the deterioration of the polarization curve.

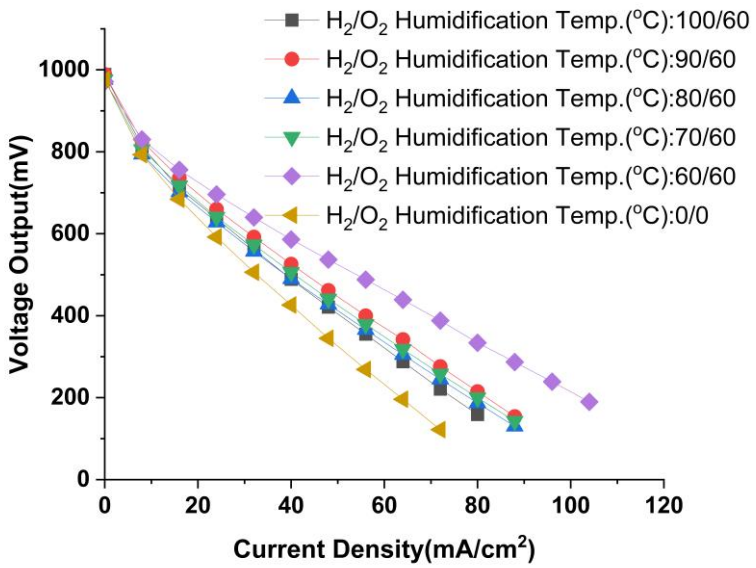

Figure 8. Voltage output for different hydrogen humidification temperatures (H_2/O_2 Humidification Temp (°C): 100/60 means that the hydrogen humidification temperature is 100 °C and the oxygen humidification temperature is 60 °C).

The voltage overpotential was determined by carefully examining the polarization curve and the voltage output data, and the values are presented in Table 5.

Table 5. Voltage overpotential and MPP for different humidification temperatures.

	Activation loss	Ohmic loss	Concentration loss	Total loss	Power at MPP	Load at MPP
Humidification temperature (°C)						
No humidification	631	223	-	854	426	40
60	579	232	-	811	532	56
70	597	298	-	895	531	56
80	610	236	-	846	514	48
90	463	184	188	832	560	56
100	568	262	-	830	506	48

In a PEMFC, the presence of water on the anode side plays a crucial role in facilitating the dissociation of hydrogen. Under varying humidification conditions, distinct effects on the cell's performance can be observed.

1. In cases with no humidification, inadequate moisture leads to high activation losses (631 mV). As depicted in Figure 8, the fuel cell can only sustain a maximum load of 72 mA/cm², indicating severely limited load-bearing capacity.
2. At a humidification temperature of 100 °C, despite achieving the lowest voltage overpotential (830 mV), the fuel cell exhibits the lowest load-bearing capacity among all tested temperatures, unable to support loads beyond 80 mA/cm².
3. Conversely, at a humidification temperature of 90 °C, which yields the most favorable results compared with other temperatures, efficient reactant utilization is achieved. However, towards the end of the channels, this optimal condition can lead to some concentration loss (188 mV) due to potential reactant depletion.

These observations underscore the critical role of water management and temperature control in optimizing PEMFCs' performance, balancing activation losses, load capacity, and reactant utilization efficiency.

Figure 9 presents the power output corresponding to various humidification temperatures. The graphs for 100 °C and zero humidification are distinctly separated from the others, indicating lower power generation. This gap widens notably beyond a load of 50 mA/cm². In contrast, the power curve for the 90 °C humidification temperature stands out on the higher power generation side compared with the majority of the curves.

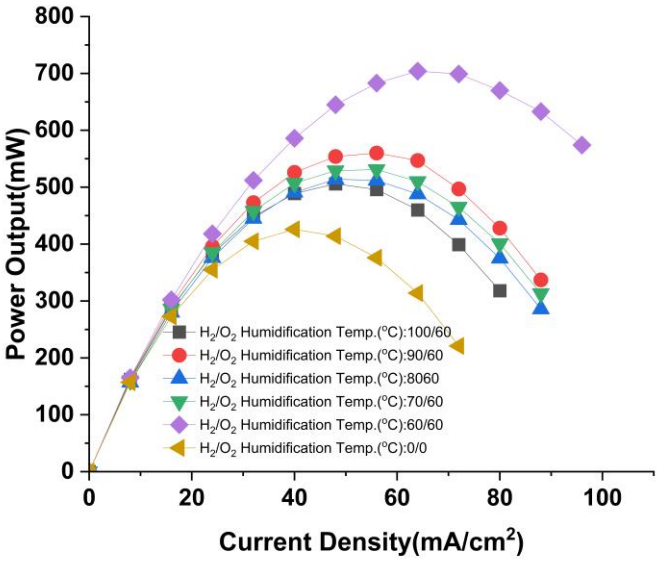

Figure 9. Power output for different hydrogen humidification temperatures (H_2/O_2 Humidification Temp (°C): 100/60 means that the hydrogen humidification temperature is 100 °C and the oxygen humidification temperature is 60 °C).

According to Table 5, at a humidification temperature of 90 °C, the maximum power output reaches 560 mW at the MPP, which also corresponds to the highest load (56 mA/cm²) among all the MPP values observed in this study.

Comparing the power at the MPP for various humidification temperatures between this study and the author's previous work with a higher catalyst loading reveals significant differences. For the lower catalyst loading, the peak power output is 36% lower at the 60 °C humidification temperature, 32% lower at 70 °C, 34% lower at 80 °C, and 24% lower at 90 °C. However, notably, under conditions of no humidification and at a 100 °C humidification temperature, the lower catalyst loading shows an improvement compared with higher catalyst loading, although these values remain the lowest among all the MPP values considered.

These findings underscore the complex relationship among humidification temperature, catalyst loading, and power generation efficiency in PEMFCs, highlighting the critical role of the experimental conditions in optimizing the performance metrics.

Overall summary

A high-performing fuel cell is expected to operate with minimal voltage overpotential, handle maximum loads, and achieve its maximum power point at higher loads. On the basis of the experiments conducted, we can conclude the following.

1. Optimal results in terms of voltage overpotential are observed at a hydrogen flow rate of 100 mL/min and excess oxygen levels of 100% and above, compared with stoichiometric oxygen requirements. These conditions also enhance the load-bearing capacity, allowing loads to exceed 88 mA/cm².
2. However, when comparing these results—specifically voltage and power output—with the best values achieved with a higher catalyst loading, they show slight inferiority. Higher

catalyst loading can produce approximately 20% more peak power than lower catalyst loading. In terms of voltage output, the voltage overpotential is about 50 mV lower with the higher catalyst loading, while still supporting loads up to 90 mA/cm².

3. The maximum power point across all hydrogen flow rates and excess oxygen levels typically spans a load range of 40–64 mA/cm². By allowing for a 10% reduction in maximum power at each excess oxygen level, the load range expands to cover values from 32 to 80 mA/cm².
4. Experimenting with varying humidification temperatures (ranging from zero humidification to 60 °C, 70 °C, 80 °C, 90 °C, and 100 °C) under conditions of a 100 mL/min hydrogen flow rate and 150% excess oxygen shows results similar to those observed with the higher catalyst loading. However, despite these similarities, the superior performance associated with the higher catalyst loading remains evident, albeit marginally.
5. Therefore, with only a marginal decrease in performance, PEMFCs can effectively operate with a lower catalyst loading, especially if coupled with a specialized flow field design. This approach underscores the potential feasibility of optimizing fuel cells' performance under varied experimental conditions.

3.5. Comprehensive comparison of performance with two different catalyst loadings

Both catalyst loadings demonstrated their best performance at a hydrogen flow rate of 100 mL/min. Figure 10A and B present the polarization curves and power curves, respectively, for this hydrogen flow rate. Both figures are drawn for varying excess oxygen supply levels at the two catalyst loadings. Although the reaction rates are lower with the reduced catalyst loading, the difference in catalyst loadings did not result in significant variations at this flow rate.

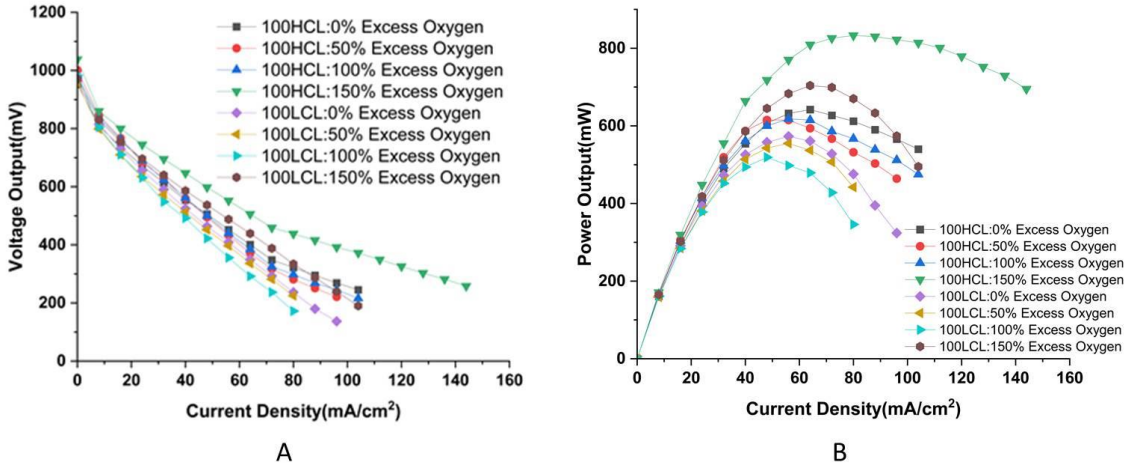

Figure 10. Comparison of performance of lower and higher catalyst loadings for the 100 mL/min hydrogen flow rate. A: Voltage output. B: Power Output (100HCL:50% Excess Oxygen: The higher catalyst loading at a 100 mL/min hydrogen flow rate and 50% excess oxygen).

Figure 10A shows that both catalyst loadings achieve higher polarization curves when supplied with 150% excess oxygen compared with all other excess oxygen supplies in their respective categories. Moreover, while reaction rates at the anode are lower for the lower catalyst loading, the 150% excess oxygen supply indicates that the anode reaction remains sufficiently high, necessitating an oxygen supply comparable with that of higher catalyst loading.

Figure 10B, illustrating power output, is consistent with the results of the polarization curve. For example, 150% excess oxygen supply yields a power output of 833 mW and 704 mW for the higher and lower catalyst loadings, respectively. The peak power outputs occur at current densities of 80 and 64 mA/cm² for the higher and lower platinum loadings, respectively, which are higher than those associated with the other maximum power points for different excess oxygen supply levels for both catalyst loadings.

Given the interest in comparing the optimal humidification temperatures for higher and lower catalyst loadings under the conditions of the most suitable hydrogen flow rate and excess oxygen supply (100 mL/min and 150% excess oxygen, respectively), experiments were conducted as outlined in Section 2. The resulting polarization curves and power output curves for various humidification temperatures are presented in Figure 11.

As illustrated in Figure 11A (polarization curves) and Figure 11B (power output curves), the curves for the lower and higher catalyst loadings are distinctly separated. The curves corresponding to the lower catalyst loading are positioned at a lower level, indicating higher voltage overpotential and reduced power output compared with those associated with higher catalyst loading across different humidification temperatures.

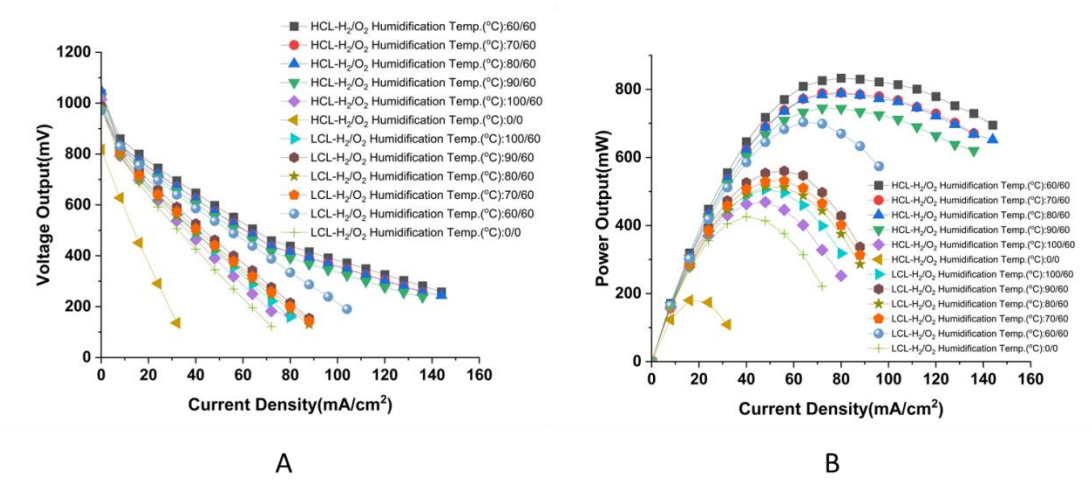

Figure 11. Voltage output and power output for different humidification temperatures. A: Voltage output; B: Power output (HCL-H_2/O_2 Humidification Temp (°C): 70/60 means 70 °C as the hydrogen humidification temperature and 60 °C as the oxygen humidification temperature for the higher catalyst loading).

Within each group, with the exception of the dry run and the 60 °C hydrogen humidification temperature, the curves for all humidification temperatures are closely grouped, indicating similar values. The absence of humidification adversely affects the performance of the fuel cell, as water

molecules are essential for proton transport. Additionally, higher cell resistance is another cause of poor performance.

The humidification temperature refers to the temperature to which water is heated in the humidifier. A higher humidification temperature results in increased vapor pressure, which leads to a disproportionately greater amount of water vapor produced. Conversely, a lower humidification temperature yields lower vapor pressure, producing a proportionately greater amount of water vapor, although still less than that generated at higher humidification temperatures. Additionally, at lower humidification temperatures, hydrogen gas can dissolve in smaller quantities. The resulting water vapor, with hydrogen dissolved in it, is then adsorbed by the platinum catalyst. This adsorption reduces the activation energy, allowing hydrogen to undergo ionization. Subsequently, the water vapor carries protons to the cathode side.

Notably, a lower humidification temperature facilitates more water vapor permeation into the membrane. Consequently, even a humidification temperature of 60 °C can yield better results than higher temperatures, as the voltage overpotential associated with this temperature is comparable with that observed with the higher catalyst loading.

Although line heating is implemented for both humidified gases, some water vapor will inevitably condense upon contact with the bipolar plates. The higher the humidification temperature—and consequently, the temperature of the water vapor—the greater the amount of condensation. This phenomenon explains the similar results observed across most humidification temperatures, regardless of the catalyst loading.

3.6. Statistical analysis for the evaluation of significant differences in power output

3.6.1. Statistical analysis for experiments with the optimum hydrogen flow rates and excess oxygen supply for two different catalyst loadings

In experiments involving the higher catalyst loading, the optimal hydrogen flow rate was determined to be 100 mL/min, based on the power output at the MPP. A statistical analysis was conducted for this hydrogen flow rate for 0%, 50%, 100%, and 150% excess oxygen supply. The power output for each excess oxygen level was individually tested for normality using the Shapiro–Wilk test at a significance level of 0.05. The resulting *p*-values were 0.002, 0.012, 0.004, and 0.000, respectively. Since these values are below the significance threshold, none of the datasets conform to a normal distribution.

Subsequently, the data were transformed to their logarithmic values, and the Shapiro-Wilk test was reapplied, yielding p-values of 0.00 for all groups. This indicates that even though the transformed data do not follow a normal distribution. Therefore, to assess significant differences among the four groups, the nonparametric test, Kruskal-Wallis test was employed. The observed k-value was 14.42, while the critical k-value was 7.815 (from the chi-squared table for df = 3). The corresponding p-value was 0.002, which is below the significance level of 0.05, indicating significant differences in the mean power output among the four groups.

To determine which groups exhibited significant differences from each other, Dunn's test was conducted for six pairs: 0%–50% excess oxygen supply, 0%–100% excess oxygen supply, 0%–150% excess oxygen supply, 50%–100% excess oxygen supply, 50%–150% excess oxygen supply, and 100%–150% excess oxygen supply. The p-values obtained for these comparisons were 0.587,

0.638, 0.009, 0.935, 0.002, and 0.002, respectively. Using Bonferroni's corrected significance level of 0.0083, it was determined that the group with the 150% excess oxygen supply exhibited significant differences from the other groups. This suggests that the variation in power output associated with this level of excess oxygen supply is attributed to the behavior of the fuel cell under these conditions. The details of the Kruskal-Wallis test and Dunn's test for both higher and lower catalyst loading are listed in Table 6.

Table 6. Significant differences between the power output of pairs of higher and lower catalyst loadings for different excess oxygen levels (at a 100 mL/min hydrogen flow rate).

	Higher catalyst loading	Lower catalyst loading	Higher catalyst loading		Lower catalyst loading	
	P-values for Kruskal-Wallis test (critical value: 7.81; K value: 14.21)	P-values for Kruskal-Wallis test (critical value: 7.81; K value: 7.26)	P-value for Dunn's test for higher loading for different pairs		P-value for Dunn's test for lower loading	
0%	0.002	0.064	0%–50%	0.587	-	-
			0%–100%	0.638	-	-
			0%–150%	0.009	-	-
50%			50%–100%	0.935	-	-
			50%–150%	0.002	-	-
100%			100%–150%	0.002	-	-
150%			-		-	
Remark	Since the p-value is less than 0.05, there is a significant difference among the four groups	Since the p value is greater than 0.05, there is no significant difference among the four groups	Based on Bonferroni's corrected significance level of 0.0083, the 150% excess oxygen level is significantly different from other groups		-	

Similarly for the lower catalyst loading, the normality test for the four different excess oxygen supply groups yielded the following p-values: 0.08, 0.031, 0.063, and 0.025. Since not all groups exhibited a normal distribution, the power output values were transformed to their logarithmic values, after which, the Shapiro-Wilk test was applied. The resulting p-values were 0.00 for all groups, indicating that the transformed values also do not conform to a normal distribution.

To determine whether any of the groups were significantly different from the others, the Kruskal-Wallis test was conducted, yielding the following results: Observed k-value = 7.26; critical k-value = 7.81; p = 0.064. Since $k_{\text{observed}} < k_{\text{critical}}$ and $p > 0.05$, there is no significant difference in the power output values among the four different oxygen supply levels. This implies that any small differences observed in power output across the various excess oxygen supplies are likely due to chance rather than the effect of the excess oxygen supplied.

On carrying out groupwise comparison of pairings of the lower and higher catalyst loading for different excess oxygen supply levels for the 100 mL/min hydrogen flow rate, the following results were obtained. The power output data for 0% excess oxygen supply yielded p-values of 0.0068 for the higher catalyst loading and 0.08 for the lower catalyst loading in the Shapiro-Wilk test. Since one of the groups does not follow a normal distribution, the Mann-Whitney test was employed to assess

significant differences. The results indicated U = 91 (with $U_{critical}$ = 50) and p = 0.07. Since the p-value is greater than 0.05, the power output values for the two groups representing the higher and lower catalyst loadings under 0% excess oxygen supply are derived from the same population, suggesting that any observed differences are due to chance.

For 50% excess oxygen supply, the normality test for the two groups returned p-values of 0.012 and 0.031, indicating a normal distribution. Upon applying a t-test (for unequal variance and unequal sample size), the results were t_{stat} = 0.725 and p = 0.476. Consulting the t-critical table (for df = 22), the t-critical value was found to be 2.08. Therefore, the two samples originate from the same population, and any differences observed are purely due to chance.

In the case of the 100% excess oxygen supply, normality testing yielded p-values of 0.014 for the higher catalyst loading and 0.06 for the lower catalyst loading. Given that one sample met the criteria for normality while the other did not, the Mann-Whitney U test was utilized. The results showed p = 0.04 and U = 77. Since the p-value is less than the significance level of 0.05, a significant difference exists between the two groups. To assess the practical significance of this difference, the rank-biserial correlation was calculated using the formula $r_{rb} = \frac{U}{(n_1 \times n_2)}$, where U is the Mann-Whitney U-statistic, and n_1 and n_2 are the sample sizes of the two groups. The resulting value of r_{rb} = 0.53 indicates a moderate positive correlation between the power outputs for the higher and lower catalyst loadings, with the higher catalyst loading yielding moderately higher power outputs.

For the 150% excess oxygen supply, the Shapiro-Wilk's test produced p-values of 0.048 and 0.025 for the higher and lower catalyst loading samples, respectively. Since both values are less than the significance level, the data do not follow a normal distribution. Consequently, the Mann-Whitney test was applied to evaluate the presence or absence of significant differences. The obtained results were U = 133 (with $U_{critical}$ = 78 from the critical value table) and p = 0.01. Since the p-value is less than 0.05, a significant difference exists between the means of the two groups, indicating that the power output generated by the fuel cell for higher and lower catalyst loadings differs significantly at this level of excess oxygen supply. The calculated value of r_{rb} = 0.5 suggests a moderate positive correlation between the power outputs of the fuel cell operating with two different catalyst loadings.

3.6.2. Statistical analysis for experiments with different humidification temperatures for two different catalyst loadings

For the higher catalyst loading, a normality test was conducted using Colab for six different humidification temperatures, namely 60 °C, 70 °C, 80 °C, 90 °C, 100 °C, and no humidification. The Shapiro-Wilk test yielded p-values of 0.00049, 0.005, 0.0061, 0.0085, 0.3182, and 0.242, respectively. Since the first four p-values are less than the significance level of 0.05, the null hypothesis is rejected, indicating that the data for humidification temperatures of 60 °C, 70 °C, 80 °C, and 90 °C do not conform to a normal distribution. Conversely, the data for 100 °C and the zero humidification condition satisfy the normality criteria.

While analysis of variance (ANOVA) is a useful method for determining significant differences among more than two groups, it assumes normality across all groups. Given that the first four groups do not exhibit a normal distribution, ANOVA cannot be applied.

Following the transformation of these data to their logarithmic values, normality was reassessed using the Shapiro-Wilk test, which produced p-values of 2.58×10^{-5}, 4.35×10^{-5},2.69×10^{-5}, and 4.4×10^{-5}. Since all these values are less than the alpha level of 0.05, the transformed data for humidification temperatures of 60 °C, 70 °C, 80 °C, and 90 °C still do not satisfy the normality test. Consequently, as ANOVA can only be applied to groups with a normal distribution, it is not suitable for identifying significant differences in the means of power output for the six different humidification conditions. Therefore, once again, a nonparametric test, specifically the Kruskal-Wallis test, was utilized.

Upon applying the Kruskal-Wallis test, the values obtained were $p = 0$ and $K = 27.2$. From the chi-squared table, the critical value was determined to be 11.07, which is less than 27.2. Additionally, the p-value is less than the alpha level of 0.05. Both results indicate that at least one group demonstrates a significant difference from the others regarding power output under different humidification conditions.

To identify which specific group(s) differ significantly from the others, Dunn's test was performed for 15 different pairs of groups. The p-values obtained were as follows: 0.382 (60–70 °C), 0.294 (60–80 °C), 0.043 (60–90 °C), 0.0001 (60–100 °C), 0.000 (60 °C–no humidification), 0.872 (70–80 °C), 0.2156 (70–90 °C), 0.002 (70–100 °C), 0.001 (70 °C–no humidification), 0.322 (80–90 °C), 0.003 (80–100 °C), 0.002 (80 °C–no humidification), 0.033 (90–100 °C), 0.012 (90 °C–no humidification), and 0.409 (100 °C–no humidification). The Bonferroni-corrected significance level was determined to be 0.0033.

Comparing the p-values with this corrected significance level reveals that the fifth and sixth groups (a 100 °C humidification temperature and no humidification) are significantly different from all other groups.

For the lower catalyst loading, a normality test was conducted using Colab for six different humidification temperatures: 60 °C, 70° C, 80 °C, 90 °C, 100 °C, and a no humidification. The Shapiro-Wilk test yielded p-values of 0.0025, 0.076, 0.083, 0.088, 0.083, and 0.204, respectively. Since the p-value for the 60 °C humidification temperature is less than the significance level of 0.05, the null hypothesis is rejected. Upon transforming the data for this humidification temperature to the logarithmic values and applying the Shapiro-Wilk test for normality, the p-value was found to be 0.0022. This value is also less than significant level. This indicates that even the transformed data do not conform to a normal distribution. Consequently, Kruskal-Wallis test was applied to assess whether there are significant differences among the six groups representing the various humidification temperatures.

The Kruskal-Wallis test gave a p-value of 0.019 and an observed K value of 13.468. From the chi-squared table, the critical value of K was found to be 11.07, which is less than the observed K value. Additionally, the p-value is less than the alpha level of 0.05, suggesting that the samples do not originate from the same population.

To identify which humidification temperatures significantly differ from one another, Dunn's test was conducted for 15 different pairs of groups. The resulting p-values for these pairs were as follows: 0.053 (60–70 °C), 0.017 (60–80 °C), 0.131 (60–90 °C), 0.019 (60–100 °C), 0.001 (60 °C–no humidification), 0.667 (70–80 °C), 0.681 (70–90 °C), 0.665 (70–100 °C), 0.125 (70 °C–no humidification), 0.400 (80–90 °C), 0.990 (80–100 °C), 0.260 (80 °C–no humidification), 0.404 (90–100 °C), 0.054 (90 °C–no humidification), and 0.275 (100 °C–no humidification). The Bonferroni-corrected significance level was established at 0.0033.

From this analysis, it can be concluded that the 60 °C humidification temperature and the zero humidification condition exhibit significant differences when compared with the other groups.

The groupwise comparison of pairings of lower and higher catalyst loadings led to the following results**.** Table 7 summarizes the statistical tests conducted to assess the presence or absence of significant differences between the readings related to the higher and lower catalyst loadings across various humidification temperatures. Notably, with the exception of the zero humidification condition, significant differences in the power output values were observed for all other humidification temperatures when comparing the higher and lower catalyst loadings.

Table 7. Significant differences between the power output of pairs of higher and lower catalyst loadings for different humidification temperatures.

	Higher catalyst loading: Test for normality		Lower catalyst loading: Test for normality		Mann-Whitney test (nonparametric test) **T-test		
	P	Null hypothesis (accept/reject)	p	Null hypothesis (accept/reject)	U (* critical value)	p	Null hypothesis (accept/reject)
60 °C humidification Temperature	0.003	Reject	0.025	Reject	133 (78*)	0.01	Reject
70 °C humidification Temperature	0.001	Reject	0.001	Reject	108 (61*)	0.00	Reject
80 °C humidification Temperature	0.000	Reject	0.083	Accept	114 (65*)	0.00	Reject
90 °C humidification Temperature	0.000	Reject	0.088	Accept	108 (61*)	0.00	Reject
100 °C humidification Temperature	0.019	Reject	0.083	Accept	66 (30*)	0.28	Reject
No humidification	0.258	Accept	0.204	Accept	-	0.006** (T-test)	Accept

For 60 °C, 70 °C, 80 °C, 90 °C, and 100 °C humidification temperatures, the null hypothesis is rejected, as seen in Table 7. This indicates that the observed differences in the mean power output between the higher and lower catalyst loadings at various humidification temperatures are solely attributable to the varying concentrations of the platinum catalyst present in the MEA. The minor differences in power output for these humidification temperatures are a result of the inherent characteristics of the MEA. In the case of the no humidification condition, where the power outputs for both the higher and lower catalyst loadings followed a normal distribution, a t-test was employed to compare the two groups. On the basis of the p-value of 0.006, it was determined that the two groups originate from the same population, indicating that there is no statistically significant difference between them. Any physical differences observed are therefore attributed to chance occurrences.

In conclusion, while for the higher catalyst loading, the variation in power output for different excess oxygen levels is significant and is due to significant differences in the power output associated with the 50%–150% and 100%–150% excess oxygen levels. Thus, operating the fuel cell at an excess oxygen level less than 150% will not have a significant difference in the performance for most excess oxygen levels. For the lower catalyst loading, there is no significant variation in the power output for the different oxygen levels and the difference is mainly due to chance. Hence, operating the fuel cell at any excess oxygen level will not make a significant difference in performance. There is significant difference in the power output values of the lower and higher catalyst loading at the 100% and 150% excess oxygen levels. That is to say, it really matters whether the fuel cell is operated with a higher or lower catalyst loading if the excess oxygen used is less than 100%.

Similarly, for different hydrogen humidification temperatures, there was a significant difference in the values of power output for the higher catalyst loading and that was mainly due to the power output values of many humidification temperatures. Hence, it is important to operate the fuel cell at the most appropriate humidification temperature. For the lower catalyst loading as well, there was a significant difference in the power output of various groups representing six humidification conditions and is mainly due to differences in the values of power output associated with the 60 °C humidification temperature and no humidification. In this case, the fuel cell may be operated at any humidification temperature more than 60 °C without having any significant difference in the power output. For all humidification temperatures except no humidification, there was a significant difference in the power out of the higher and lower catalyst loadings. Thus, operating the fuel cell with no humidification will not make much of a difference in the power output whether the fuel cell is operated with a higher or lower catalyst loading.

3.7. Impact on commercialization

The findings of this study hold significant practical implications for the commercialization of fuel cells utilized in low-power appliances. A primary factor contributing to the high costs of fuel cells is the membrane, largely due to its reliance on platinum catalysts. Although efforts to identify alternatives to platinum are ongoing, it remains a critical component of fuel cells. In this regard, selection of a flow field design that minimizes platinum usage while maintaining comparable performance levels would be advantageous.

The twin inlet-outlet flow field investigated in this study provides valuable insights into the potential cost savings associated with reduced platinum usage and its effect on fuel cells' performance. This information is essential for assessing the viability of commercializing fuel cell technology.

The cost of a fuel cell is directly related to the amount of platinum catalyst used, assuming that all other factors remain constant. Platinum is currently priced at approximately $1,200 per ounce. In this study, the platinum loadings were 0.20 mg/cm² at the anode and 0.4 mg/cm² at the cathode, resulting in a total platinum cost of $1.16. In contrast, our previous research with higher platinum loadings (0.25 mg/cm² and 0.5 mg/cm² for the anode and cathode, respectively) yielded a platinum cost of $1.45, indicating a 20% cost saving with the lower loading.

With the higher platinum loading, the maximum power output achieved was 833 mW, whereas the lower loading resulted in a maximum power output of 704 mW. Assuming a membrane lifespan of

1000 hours, the total revenue from the energy produced at a rate of \$0.30 per kWh is \$0.24 for the higher loading and \$0.21 for the lower loading, reflecting a revenue reduction of approximately 12.5% for the lower platinum loading. To summarize the study, it can be stated that for the lower catalyst loading, a 20% reduction in cost results in a 12.5% reduction in revenue when compared with the higher catalyst loading. Since the reduction in cost is more than the reduction in benefit, the lower catalyst loading can still be considered for operating a fuel cell at the concentration considered in this study. It is important to highlight that the maximum power outputs are recorded under higher current density loads. Typically, low-power appliances operate at relatively low loads most of the time, suggesting that the revenue difference in such scenarios would be considerably smaller.

4. Conclusions

The objective of the study was to evaluate whether the use of a lower catalyst loading in the MEA results in similar performance to that of a specific higher catalyst loading when a special type of flow field is used in a PEMFC. On the basis of the findings presented and the discussion conducted, the following conclusions are drawn:

1. The fuel cell with the special flow field operates effectively at a lower catalyst loading compared with those seen with the higher catalyst loading.
2. The lowest voltage overpotential is observed at a hydrogen flow rate of 100 mL/min and 150% excess oxygen supply. In contrast, the higher catalyst loading achieves optimal performance at the 80 mL/min hydrogen flow rate and 75% excess oxygen supply. This suggests that with the specific flow field used in this study, there is a slight economic advantage to using the higher catalyst loading in terms of operational costs.
3. The maximum power point generally shifts towards higher loads and increases with a higher excess oxygen supply in most cases. However, beyond a certain excess oxygen supply, typically beyond 100%, there is a reduction in maximum power.
4. The maximum power points across various hydrogen flow rates and excess oxygen supplies range between 40 and 64 mA/cm². Allowing for a 10% reduction in maximum power expands the covered load range to 32–80 mA/cm².
5. Optimal values for voltage output, maximum power output, and cell resistance are achieved with a hydrogen flow rate of 100 mL/min and an excess oxygen supply of 150%.
6. The performance parameters for the lower catalyst loading are marginally inferior to those achieved with the higher catalyst loading, demonstrating that comparable performance can be attained with the lower catalyst loading when using the specialized flow field employed in this study.
7. The lower catalyst loading exhibits considerable cell resistance even at lower loads compared with the higher catalyst loading. Specifically, cell resistance starts from 4 mA/cm² for the lower catalyst loading, whereas it begins at 6 mA/cm² for the higher catalyst loading across experiments conducted at various humidification temperatures.
8. A notable finding is the absence of concentration loss observed with the lower catalyst loading, contrasting with the significant concentration loss observed with the higher catalyst loading under similar conditions.

These conclusions highlight the potential viability of utilizing lower catalyst loadings in PEMFCs, especially when complemented with a specialized flow field design, despite slight trade-offs in the performance parameters compared with higher catalyst loading scenarios.

Use of AI tools declaration

No AI tools were used in the preparation of this paper.

Acknowledgment

This work was supported by the All India Council for Technical Education (AICTE) grant funded by the Government of India (No.8-168/FDC/RPS(Rural)/POLICY-1/2021-22) and NMAM (Nitte Mahalinga Adyanthaya Memorial) Institute of Technology (NITTE—deemed to be a university). The authors give profuse thanks for the support provided by the two organizations.

Conflict of interest

The authors declare that they have no known competing financial interests or personal relationships that could have appeared to influence the work reported in this paper.

References

1. Agyekum EB, Ampah JD, Wilberforce T, et al. (2022) Research progress, trends, and current state of development on pemfc-new insights from a bibliometric analysis and characteristics of two decades of research output. *Membranes* 12: 1103. https://doi.org/10.3390/membranes12111103
2. Agyekum EB, Nutakor C, Agwa AM, et al. (2022) A critical review of renewable hydrogen production methods: Factors affecting their scale-up and its role in future energy generation. *Membranes* 12: 173. https://doi.org/10.3390/membranes12020173
3. Wang Y, Chen KS, Mishler J, et al. (2011) A review of polymer electrolyte membrane fuel cells: Technology, applications, and needs on fundamental research, *Appl Energy* 88: 981–1007. https://doi.org/10.1016/j.apenergy.2010.09.030
4. Solis BP, Cruz Argüello JC, Gómez BL, et al. (2019) Bibliometric analysis of the mass transport in a gas diffusion layer in PEM fuel cells. *Sustainability* 11: 6682.
5. Ning F, Zhu X, Liu Y, et al. (2024) High safety fuel cells based on gas diffusion layer suppressed uneven current and thermal runaway. *Adv Funct Mater* 35: 2414081. https://doi.org/10.1002/adfm.202414081
6. Sauermoser M, Kizilova N, Pollet BG, et al. (2020) Flow field patterns for proton exchange membrane fuel cells. *Front Energy Res* 8: 13. https://doi.org/10.3389/fenrg.2020.00013
7. Suresh PV, Jayanti S, Deshpande AP, et al. (2011) An improved serpentine flow field with enhanced cross-flow for fuel cell applications. *Int J Hydrogen Energy* 36: 6067–6072. https://doi.org/10.1016/j.ijhydene.2011.01.147

8. Zhou Y, Meng K, Chen W, et al. (2023) Experimental performance of proton exchange membrane fuel cell with novel flow fields and numerical investigation of water-gas transport enhancement. *Energy Convers Manage* 281: 116865. https://doi.org/10.1016/j.enconman.2023.116865
9. Suarez C, Iranzo A, Toharias B, et al. (2022) Experimental and numerical Investigation on the design of a bioinspired PEM fuel cell. *Energy* 257: 124799. https://doi.org/10.1016/j.energy.2022.124799
10. Wen Q, He C, Ning F, et al. (2024) Engineering highly efficient root-inspired microporous layer for high-performance fuel cells. *Chem Eng J* 497: 154424. https://doi.org/10.1016/j.cej.2024.154424
11. Wang Y, Wang L, Ji X, et al. (2021) Experimental and numerical study of proton exchange membrane fuel cells with a novel compound flow field. *ACS Omega* 2021 6: 21892–21899. https://doi.org/10.1021/acsomega.1c01924
12. Kahraman H, Orhan MF (2017) Flow field bipolar plates in a proton exchange membrane fuel cell: analysis & modeling. *Energy Convers Manage* 133: 363–384. https://doi.org/10.1016/j.enconman.2016.10.053
13. Alabi AS, Popoola API, Popoola OM, et al. (2023) Materials for electrocatalysts in proton exchange membrane fuel cell: A brief review. *Front Energy Res* 11: 1091105. https://doi.org/10.3389/fenrg.2023.1091105
14. Liu Y, Tian B, Ning F, et al. (2023) Hybrid 3d-ordered membrane electrode assembly (MEA) with highly stable structure, enlarged interface, and ultralow ir loading by doping nano TiO_2 nanoparticles for water electrolyzer. *Adv Energy Mater* 14: 2303353. https://doi.org/10.1002/aenm.202303353
15. Sammes N (2006) Fuel cell technology—reaching towards commercialization. Spinger—Verlag, London. https://doi.org/10.1007/1-84628-207-1
16. Allwyn Blessing Johnson N, Sen AK, Das SK (2023) Effect of humidification and cell heating on the operational stability of polymer electrolyte membrane fuel cell. *Int J Hydrogen Energy* 48: 35267–35279. https://doi.org/10.1016/j.ijhydene.2023.05.269
17. Chen X, Wang C, Xu J, et al. (2023) Membrane humidity control of proton exchange membrane fuel cell system using fractional-order PID strategy. *Appl Energy* 343: 121182. https://doi.org/10.1016/j.apenergy.2023.121182
18. Hung AJ, Sung LY, Chen YH, et al. (2007) Operation-relevant modeling of an experimental proton exchange membrane fuel cell. *J Power Sources* 171: 728–737. https://doi.org/10.1016/j.jpowsour.2007.06.066

AIMS Press